Journal of Environmental Chemical Engineering 5 (2017) 432–441

Contents lists available at ScienceDirect

Journal of Environmental Chemical Engineering

journal homepage: www.elsevier.com/locate/jece

Vitrification of hazardous Fe-Ni wastes into glass-ceramic with fine crystalline structure and elevated exploitation characteristics

Alexander Karamanov[a,*], Perica Paunović[b], Bogdan Ranguelov[a], Ejup Ljatifi[b], Alexandra Kamusheva[a], Goran Načevski[b], Emilia Karamanova[a], Anita Grozdanov[b]

[a] Institute of Physical Chemistry, Bulgarian Academy of Sciences, Sofia, Bulgaria
[b] Faculty of Technology and Metallurgy, SS Cyril and Methodius University, Skopje, Republic of Macedonia

ARTICLE INFO

Article history:
Received 18 August 2016
Received in revised form 28 November 2016
Accepted 17 December 2016
Available online 19 December 2016

Keywords:
Iron-reach glass-ceramic
Structure
Pyroxenes
Mechanical properties

ABSTRACT

Hazardous residues from ferronickel smelting plant are mixed with glass cullet and are vitrified for 2 h at 1400 °C. The obtained glass is characterized with a very high crystallization trend. As a result, it is inappropriate for sinter-crystallization, but a fine crystalline glass-ceramic can be obtained by bulk crystallization after short heat-treatment at low temperatures.

Due to the presence of 1.5 wt.% chromium oxide in the parent glass, together with high amounts of iron oxides and magnesium oxides, the crystallization process is peculiar. It starts during the melt cooling with the precipitation of preliminary Fe-Mg-Cr spinel crystals, which then act as centers for further epitaxial growth of pyroxene phase. It is also highlighted that, due to liquid–liquid immiscibility, the main amorphous phase is characterized by a nonhomogeneous binodal structure, which becomes finer after the nucleation treatment. As a result, pyroxenes with sizes below 1 μm are formed as main crystal phase after the crystallization step.

Notwithstanding of the high amount of hazardous wastes in the batch the obtained glass is characterized with high chemical durability. At the same time, the obtained glass-ceramics is characterized by a suitable coefficient of thermal expansion and attractive mechanical characteristics.

1. Introduction

During the vitrification of hazardous inorganic industrial wastes the harmful metals are bonded chemically in a stable amorphous structure [1–4], which drastically decreases their solubility. However, this advanced technique for immobilization has a relatively high cost and its application is justifiable mainly when it is difficult to use cheaper methods for waste inertization or/and when materials with added value can be obtained. From this point of view, the synthesis of glass-ceramics seems to be one of the most promising solutions. In fact, huge number of studies, related to glass-ceramic by different harmful wastes, carries out each year [5–13]. A significant part of these publications is related to different iron-rich compositions [14] arising from the hydro-metallurgy of zinc ores [15–19], electric arc furnace dusts [20], wastes from Cu flotation [21,22], MSWA [23] and other residues [24]. Some of these compositions are somewhat similar to basalt rocks used in the petrurgy (fused rocks industry) [25,26] or to glasses used for vitrification of wastes from nuclear power stations [1,27,28].

The iron-rich glasses have some interesting peculiarities, which decrease both the costs of glass melting and crystallization heat-treatment. Probably, this is another reason for the interest toward these compositions.

Firstly, the iron-rich compositions are characterized by specific viscosity curves, which at the same time are characterized by relatively high glass-transition temperatures (which indicates a good chemical durability) and by low melting temperatures. The “melting points” (i.e. the temperatures corresponding to a viscosity of 10^2 dPa s) in a typical iron-rich glass forming melt occurs at significantly lower temperature (by 150–200 °C), than the temperatures for melting of container glass or traditional glass-ceramics from wastes [29–32]. This sharp drop of viscosity at high temperatures can be related to changes of melt structure with the temperature, caused by the high amount of iron oxides in the melt.

The lower melting temperature leads to a significant decreasing of the price of vitrification procedure. At the same time, the tendency for evaporation of heavy metals during the glass melting

* Corresponding author.
E-mail address: karama@ipc.bas.bg (A. Karamanov).

http://dx.doi.org/10.1016/j.jece.2016.12.020
2213-3437/

diminish at lower temperatures, which is another advantage when iron-rich hazardous wastes are vitrified.

The crystallization process in the iron-rich glasses also is particular. Usually in similar compositions a tendency for liquid–liquid immiscibility at higher temperature is presented, which leads to the separation of an iron-rich phase during the cooling; then these zones very fast crystallizes into magnetite spinel [17,18,21,33,34]. It is interesting to note that during a subsequent nucleation heat-treatment in the glass transition range the number of thus formed spinel crystals doesn't change significantly. As a result, similar iron-rich glass-ceramics can be obtained by a single crystallization step.

However, when Cr_2O_3, TiO_2, CaF_2 or/and high amount of MgO are presented in an iron-rich glass, the phase formation processes become more complex [11,17,35,36] and sometimes the classical nucleation treatment becomes efficient. This is a premise for formation of a very fine-crystalline structure and enhanced mechanical properties.

The chromium oxide is considered as a traditional nucleation agent for the pyroxene glass-ceramics and its optimal concentration usually is at about 0.7–1 wt%. Its activity, similarly to one of the iron oxides, is related to the formation of tiny spinel crystals, which then promote epitaxial growth of the main pyroxene phase.

In silicate melts Cr_2O_3 is characterized with a low solubility, which value depends on the glass composition and the oxygen fugacity [37–39] and which falls with the decreasing of temperature. As a result, when the initial chromium concentration is superior of 1–2 wt.% a part of its oxide precipitates into "preliminary" spinel crystals at high temperatures [17,35,36]. It could be assumed that this precipitation takes place mainly during the cooling of the melt in the temperature interval between 1200 and 900 °C. The remaining part of Cr_2O_3 participate in the formation of "secondary" magnetite spinel at low temperatures and prolonged heat-treatment.

It is known also that the chromium oxide significantly decreases the surface tension of the silicate melts [31,39,40]. This means that it could influence the liquid–liquid separation and/or directly could decrease the thermodynamic barrier for nucleation [40]. In fact, the presence of oxides as MoO_3, WO_3 and V_2O_5, which decrease the surface tension, often leads to the formation of fine crystalline glass-ceramics [40,41]. Since the immiscibility is a typical feature for the iron-rich glasses these possibilities also can be taken into considerations.

The studied in this work glass is characterized with elevated amounts of MgO and iron oxides. In addition, it contains ~1.5% Cr_2O_3. As a result, this composition is characterized together with a tendency for liquid–liquid immiscibility and a high crystallization trend. The main aim of this work is to highlight the peculiarities of this particular phase formation process, as well as to elucidate the proposed in a previous work [42] low-cost crystallization heat-treatment for production of bulk glass-ceramic.

The previous study was based on the evaluation of the optimal crystallization heat-treatment by using DTA and pycnometric methods, while the main aim of present work is to elucidate the phase evolution and the structure of obtained glass-ceramic by detailed SEM observations.

At the same time, since the parent batch is based on huge amount of hazardous wastes, the chemical durability of obtained glass and glass-ceramics are studied, together with the main properties of the glass-ceramic.

2. Characteristics of the used waste products

The used metallurgical wastes originate from the ferronickel smelting plant FENI INDUSTRY, Kavadarci region–Republic of Macedonia. The principal technological line of the plant is schematically presented in Fig. 1. The first stage of the manufacture cycle is pre-reduction of the used ores; it is carried out in rotation kiln and yields filter dust as a waste. During the next stage of reductive smelting, together with the crude ferro-alloy an electro-furnace slag is created, which is the main waste stream of this production. In the last stage of manufacture, during the refinement of final ferro-nickel alloy in a converter, another type of slag is formed. The annual amounts of theses streams, according to the manufacturer report for 2012–2013 [42], are: filter dust (FD)–102,000 tons, slag from electro-furnace (SEF)–1 135,000 tonsand slag from converter (SC)–109,000 tons.

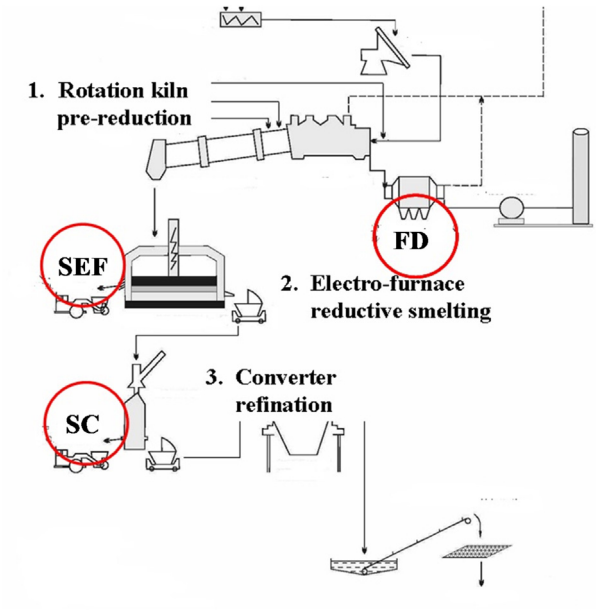

Fig. 1. Scheme of the technological line of FENI INDUSTRY, Kavadarci.

The chemical compositions of the corresponding waste materials are determined by X-ray fluorescence (XRF) spectrometer (Model XRF ARL 9900) and the results are presented in Table 1. The samples for XRF analysis were prepared by the following procedure: the mixture of 0.2 g of the each waste material and 10.4 g of sodium tetraborate as a flux was melted at 1200 °C, casted in platinum mold obtaining the sample for XRF analysis. For each waste material, three samples for three parallel measurements were prepared.

The main SEF waste is rich of silica, iron oxides and MgO, which indicate that it is an attractive material for further vitrification treatment. Somewhat similar are the characteristics of the FD residue, while SC waste is mainly composed by iron oxides with some CaO and MgO.

Table 1
Chemical compositions (wt%) of used filter dust (FD), slag from electro-furnace (SEF), converter slag (SC), container glass (CG) and obtained parent glass (G) [42].

	FD	SEF	SC	GR	G
SiO_2	37.5 ± 0.4	53 ± 0.5	1.9 ± 0.01	71.4	55
MgO	14.5 ± 0.1	16.9 ± 0.1	6.2 ± 0.1	3.3	12.1
CaO	2.3 ± 0.02	2.4 ± 0.02	15.9 ± 0.1	9.8	5.4
Al_2O_3	1.8 ± 0.01	2 ± 0.01	0.3 ± 0.01	0.6	1.5
Cr_2O_3	1 ± 0.01	2.5 ± 0.02	0.7 ± 0.01		1.5
CoO	0.1 ± 0.01	0.1 ± 0.01	0.1 ± 0.01		0.1
NiO	2.7 ± 0.02	0.1 ± 0.01	0.45 ± 0.01		0.2
Fe_2O_3	30 ± 0.3	14 ± 0.1	60 ± 0.5		19.8
FeO		9 ± 0.1	19 ± 0.2		–
Na_2O				13.3	4
K_2O				1.3	0.4

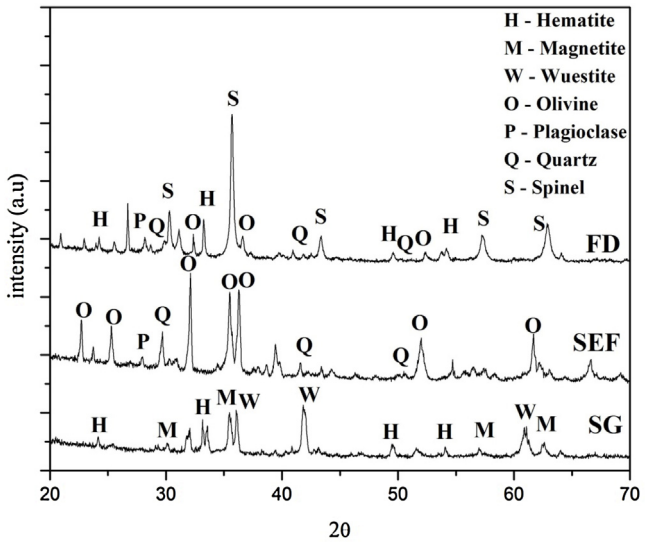

Fig. 2. XRD spectra of the waste materials.

Mineralogical analysis is carried out by X-ray diffraction method (Philips APD 15 diffractometer), operating at CuKα-radiation. The diffraction data are collected at a constant rate of $0.02^\circ\,s^{-1}$ over an angle range of 2θ from 5 to 90°. The obtained spectra are presented in Fig. 2. According to the XRD analysis, the main phases in SEF and DF are various silicates (mainly olivine, plagioclase and quartz), while in SC different iron oxides are formed. All these crystal phases are typical for the applied high temperature production treatments. This also is an advantage for eventual vitrification, because dense and no-foaming glass batch could be obtained.

The environmental impact of the studied wastes was estimated by a standard Toxicity Characteristic Leaching Procedure (TCLP) leaching test for 24 h at pH = 5.0 ± 0.2, controlled by 0.5 M solution of acetic acid and by using 100 g samples for each waste. The concentrations of heavy metals in the obtained solution after the test are measured by atomic absorption spectroscopy (AAS) using Perkin Elmer AA400 and the results are summarized in Table 2. The measured values for several metals exceed the permissible limits for not hazardous wastes [43], which demonstrate that these residues cannot be landfilled and can be considered as harmful residues. Metals as Ni, Zn and As are the hazardous elements in the dust, Ni and Cr – in the electric-furnace slag and the converter slag. The extremely high concentration of iron in the solutions of SEF and SC also can be taken into consideration.

Table 2
Concentration of the heavy metals in the solution after TCLP test (mg^*l^{-1}).

	FD	SEF	SC	G	GC	Applied limits [43]
Fe	1	202	1155	0.416	0.26	
Ni	6.1	2.7	19.2	0.311	0.1	1
Co	0.4	0.14	1.1	<0.005	<0.005	2
Cd	<0.005	<0.005	<0.005	<0.005	<0.005	0.02
Cu	0.15	0.093	0.07	0.011	0.042	5
Mn	4.7	14.6	1.5	<0.005	<0.005	
Pb	0.026	0.031	0.086	0.017	<0.005	1
Zn	3.6	0.29	0.42	<0.005	0.006	5
Cr	0.22	1.1	2.9	<0.005	<0.005	1.0
As	1.2	0.011	0.18	0.009	0.003	0.2

3. Experimental

The parent batch is obtained by mixing and homogenization of the three wastes SEF, FD and SC in proportion 10/1/1, which practically corresponds to the ratio arising from the production cycle [42]. Then, 30 wt.% container glass, crashed bellow 5 mm, is mixed with 70 wt.% of thus obtained waste mixture. The chemical compositions of glass cullet, CG, and obtained glass, G, also are reported in Table 1.

Similar approach gives a possibility for entire use of the considered industrial streams, as well as for a very cheap batch, based only on waste products. The addition of glass cullet is a common method used at the synthesis of similar glass-ceramics [1–3]; it favors the glass melting, improves the chemical durability and decreases the crystallization trends. Actually, due to the elevated percentage of MgO, iron oxides and Cr_2O_3, the direct vitrification of the main SEF residue or of the parent waste mix is unsuitable, because it will produce a glass with extremely high crystallization trend and lower chemical durability.

After additional homogenization, 300 g batch is melted in 200 ml corundum crucible using lift super-kanthal furnace. The main part of the batch is put in the crucible at room temperature, while the remaining part is added during a temperature step at about 1200 °C. Then the temperature is increased up to 1400 °C and after 2 h holding, the resulting melt is quenched in a cupper casting mold. As a result, 15–20 cm glass bars are obtained, which after annealing and crystallization treatments are cut into (4.5–5.5)/(0.9.–1)/(0.6–0.7) cm specimens, appropriated for evaluation of thermal and mechanical properties. Small glass bulk pieces with weight of about 2–3 g are also cut and heat-treated at different nucleation and crystallization times. These samples are used for evaluation of the crystallinity [42] and for topography observations with scanning electron microscope (SEM).

The appropriate method for glass-ceramic production (i.e. bulk crystallization or/and sinter-crystallization), applicable for thus obtained glass, was selected after preliminary tests. The crystallization ability is estimated by Simultaneous DTA-TG analysis (Perkin Elmer-Diamond) runs in air at $20\,^\circ C\,min^{-1}$ using bulk and powder (<75 μm) samples with weight of 15–20 mg. The sinterability is evaluated by hot stage microscopy, HSM (Misura–HSM 1400) using the same glass powder at the same heating rate.

The phase formation in samples, heat-treated at different crystallization regimes, is studied in details by SEM (JEOL JSM 6390) with INCA energy dispersive x-ray spectrometer. The apparatus is equipped with scanning system in regimes of secondary electron image (SEI) and back scattered electron (BEC) mode. Before the observations the samples were grinded and polished, etched in 2% HF solution for 3 s and coated with Au.

The XRD spectra of the powdered parent glass sample and final glass-ceramic were obtained by Philips PW 1050 diffractometer, equipped with Cu Kα tube and scintillation detector. X-ray powder diffraction patterns were recorded in the angle interval 10–70° (2θ) at steps of 0.03° (2θ) and counting time of 3 s/step.

Different characteristics of the final glass-ceramic, obtained after optimal nucleation and crystallization heat-treatments, are measured and discussed. The density is obtained by gas pycnometer (AccyPyc 1330). The thermal expansion in the interval 20–400 °C is measured at 5 °C/min by optical dilatometer (Misura HOD 1400).

Mechanical properties such as compressive and bending strength were determined by universal strength testing set SHIMADZU AGS-X with load of 10 kN, connected with supporting software TRAPEZIUM X. The measurements were performed with a 0.5 $mm^*\,min^{-1}$ crosshead speed, using specimens for bending strength with dimensions of 5 × 5 × 50 mm, and for compressive strength 5 × 5 × 5 mm. The Vickers hardness was determined using

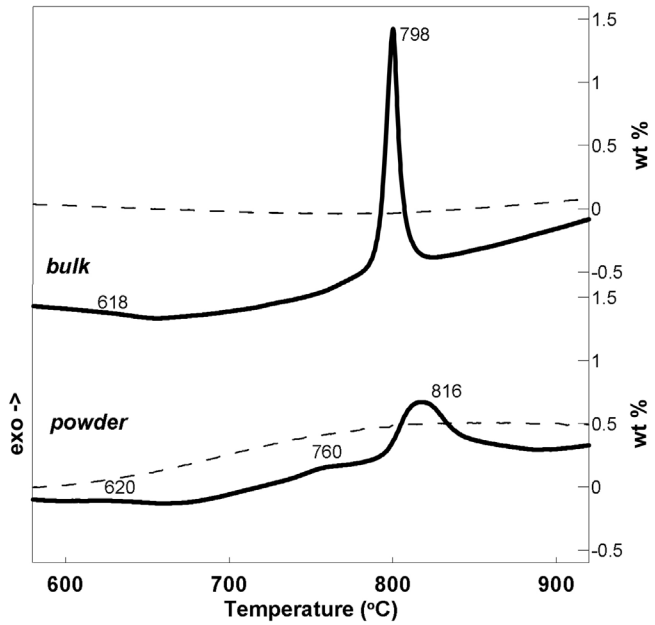

Fig. 3. DTA (solid lines) and TG (dashed lines) curves of powder and bulk glass samples.

hardness tester AVERY 6460 supplied with optical microscope [44]. The indentation was obtained with a load of 5 kg for 10 s and the Vickers hardness (HV) was calculated using Eq. (1):

$$HV = \frac{1,854 \cdot F}{d_1 \cdot d_2} \quad (1)$$

where F is the applied load and d_1 and d_2 are the diagonals of the Vickers indentation mark. The cracks that originated from the Vickers indentations were used to determine the fracture toughness using Eq. (2), proposed by Lawn and Fuller [45]:

$$K_{IC} = 0,0824 \cdot \frac{F}{c^{\frac{3}{2}}} \quad (2)$$

where *c* is an average length of the cracks obtained in the tips of the Vickers marks (microns).

Finally, the chemical durability of the obtained glass and glass-ceramic also were evaluated by TCLP test.

4. Results and discussion

4.1. Crystallization trend and sinter-ability

The DTA-TG results of bulk and powder samples of the parent glass are shown in Fig. 3. The DTA analysis highlights a glass transition at about 615–620 °C for both samples, crystallization peaks at 798 and 816 °C and enthalpies of ~85 and ~50 J g^{-1} for the bulk and powder samples, respectively. These results demonstrate that the crystallization in the bulk sample is carried out at lower temperature and leads to a formation of higher amount of crystal phase.

In addition, the traces of powder sample elucidate also a low intensity exo-therm bulge in the interval 720–780 °C, which is related to a weight gain of about 0.5 wt.%. Similar effects are attributed to the surface oxidation of Fe^{2+} into Fe^{3+}, which takes place before the crystallization and leads to variations in the kinetics of phase formation and the ratio between the formed crystal phases [19]. The main reason is the significant decreasing of the magnetite ($FeO{\cdot}Fe_2O_3$) solid solutions after the transformation of FeO into Fe_2O_3. Due to the low specific surface, analogous DTA peaks and TG gains are not observed in bulk samples.

Since in a powdered glass a whole oxidation of the iron oxides is expected near the glass transition temperature and considering that the oxidation gain for 1 wt.% FeO is 0.11%, by the TG variation it is possible to estimate the initial ratio Fe^{2+}/Fe^{3+} [23,46]. Thus obtained FeO/F_2O_3 ratio of about 1/3 for the studied glass is a typical result for similar compositions and melting procedures and indicates that at bulk crystallization spontaneous formation of iron spinels can be expected [19,47]. At the same time, the decreased crystallization trend of the glass powders, after the FeO oxidation, might favor the sinter-crystallizations.

Since the densification and the phase formation take place in same temperature interval, the sinter-ability strongly depends on the crystallization trend of used glass powder. When the crystallization rate is low the densification completes before the formation of a notable amount of crystal phase, so that sintered glass-ceramics are obtained at low temperatures (i.e. at 700–800 °C for typical iron-rich compositions) [48]. When the crystallization ability is moderate, the sintering is partially inhibited in the crystallization interval. In this case well sintered materials can be obtained after a secondary sintering near the liquids temperatures (usually at 1050–1100 °C) [23,48]. Finally, when the crystallization trend is very high, the sinter-

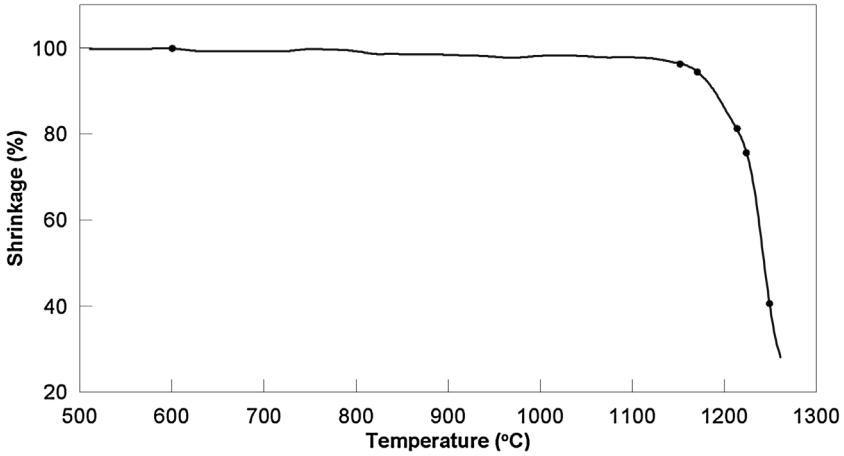

Fig. 4. HSM sintering plot.

crystallization is inappropriate because the sintering interval becomes very narrow and is shifted at higher temperatures [48].

The sinter ability of studied glass powders was tested by Hot-Stage Microscopy (HSM) experiment. This technique combines the tools of microscopy and thermal analysis by observation of a small sized pressed powder sample at a certain thermal cycle. During this measurement series of photos are recorded, which gives information about the changes in dimension and shape with temperature. As a result, the sintering interval might be estimated by measuring the shrinkage of the sample, while after the subsequent start of deformation and melting the variations in its shape can be used to obtain information for the apparent viscosity [49,50]. This is possible, because some fixed viscosity values can be related to different "characteristic forms": sintering point–10^{10} P, softening point–$10^{8.2}$ P, sphere point–$10^{6.1}$ P and half sphere point–$10^{4.6}$ P.

The results for the variations of sample's height vs. temperature are plotted in Fig. 4, whereas selected HSM photos, including ones for the observed sintering point, deformation point and half sphere are shown in Fig. 5. It is interesting to note that during the test the sample does not "pass" through a sphere shape. Similar behavior usually is observed when in the corresponding viscosity range some unmelted crystal phase yet is presented in the sample.

The sintering plot, as well as the comparison of HSM images, made at 600 °C (before the glass transition region) and at 1150 °C show that in this interval the shrinkage is less than one percent, which elucidates a very scarce sinter-ability. The densification practically starts at 1170–1180 °C and finishes after only 20–30 °C. At 1210–1220 °C deformation is observed and at 1240–1250 °C the viscosity already drops to $\sim 10^{4.6}$ P.

These results demonstrate that the densification practically takes place together with the melting of the formed crystal phases. This explains the very narrow sintering interval and indicates that serious technological problems can be expected at eventual production by high temperature sinter-crystallization. As a result, this method was abandoned and studies only with glass-ceramic, obtained by bulk crystallization, were made.

The optimal heat-treatment for manufacture of the bulk glass-ceramic was estimated in a previous study [42]. The nucleation step was evaluated by DTA analysis, while the crystallization step–by pycnometric measurements. It was highlighted that a suitable crystallization heat-treatment can be based on 45–60 min

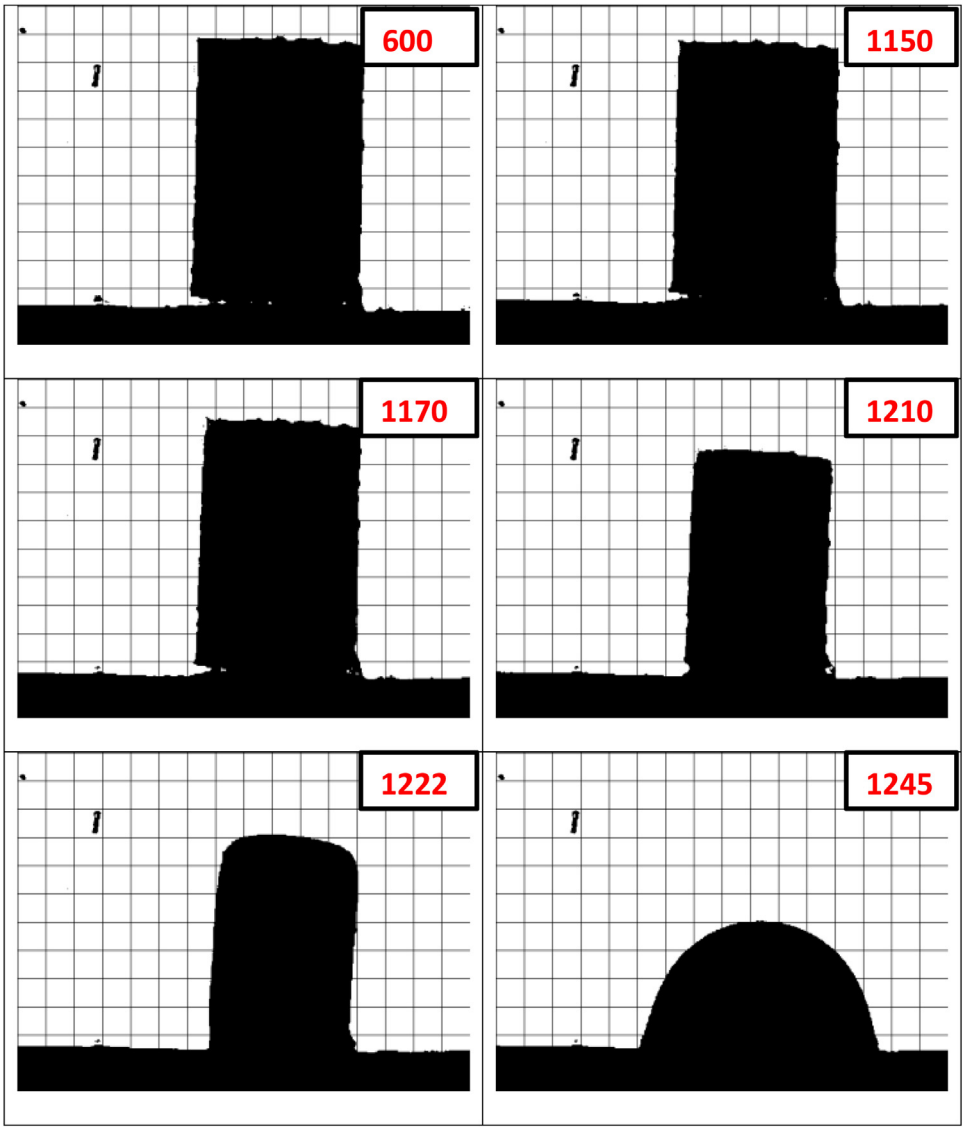

Fig. 5. HSM images at 600 °C, 1150 °C, 1170 °C (sintering point), 1210 °C, 1222 °C (softening point) and 1245 °C (half sphere point).

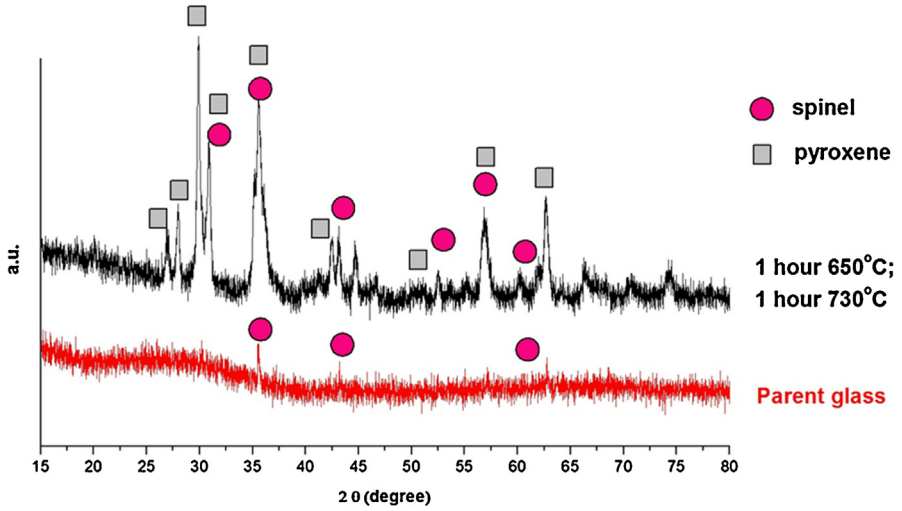

Fig. 6. XRD spectra of the parent glass and final glass-ceramic.

nucleation at about 650 °C and 30–60 min crystallization at about 730–750 °C. Similar short and low temperature heat-treatment usually is untypical for the manufacture of waste glass-ceramics [1–3] and can be considered as a positive result. The total crystallinity was estimated about 55–60%, which is a high amount for the typical iron-rich glass-ceramics. The additional kinetics valuations, made by DTA, elucidate that three dimensional crystalline structure can be expected [42].

The XRD spectra of the initial glass sample and the final glass-ceramic are presented in Fig. 6. These results confirm that the crystallization starts with the formation of some spinel phase during the melt quenching, followed by a pyroxene growth.

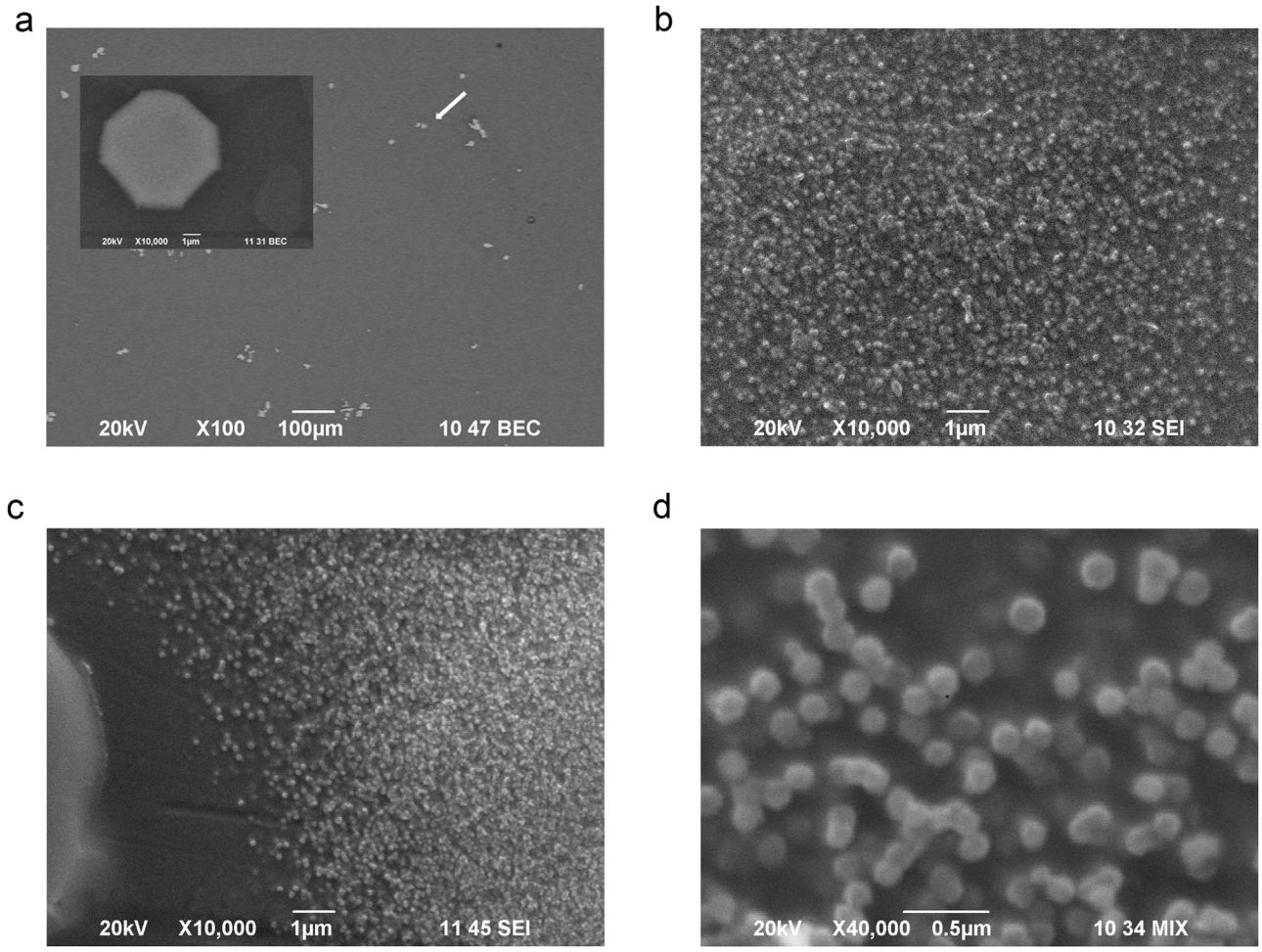

Fig. 7. SEM images after 1 min crystallization at 730 °C (***a*** and ***b*** – sample $GC_{0\text{-}1}$; ***c*** and ***d*** –sample $GC_{60\text{-}1}$).

4.2. Phase formation and structure

The efficiency of proposed nucleation treatment and the development of glass-ceramic structure were studied by scanning electron microscopy (SEM) and energy-dispersive elemental analysis (EDS). Different samples, obtained with and without nucleation step of 1 h at 650 °C and with crystallization treatments for 1, 5 and 60 min at 730 °C were prepared and analyzed. These specimens were labeled $GC_{0\text{-}1}$, $GC_{0\text{-}5}$, $GC_{0\text{-}60}$, $GC_{60\text{-}1}$, $GC_{60\text{-}5}$ and $GC_{60\text{-}60}$, where the first and the second numbers indicate the nucleation and the crystallization time, respectively. The crystallinity of the samples was evaluated by density measurements [42] and the results show that after 1 min at 730 °C the formed crystal phase is 6 ± 3% for both $GC_{0\text{-}1}$ and $GC_{60\text{-}1}$ samples. After 5 min crystallization treatment the crystallinity increases up to 10 ± 3 and 21 ± 3% for $GC_{0\text{-}5}$ and $GC_{60\text{-}5}$, respectively, while 43 ± 3% and 50 ± 3 crystal phase was measured for samples $GC_{0\text{-}60}$ and $GC_{60\text{-}60}$.

Since after 1 min at 730 °C the phase formation is in its initial stage, the SEM observations practically elucidate only the formation of the preliminary spinel crystals. Their size is estimated between 3 and 10 μm for both $GC_{0\text{-}1}$ and$GC_{60\text{-}1}$ samples. The distribution of these spinel into the main glassy matrix is shown in Fig. 7a; in the inset of figure is presented a typical single crystal at higher magnification. The EDS analysis of these preliminary spinel crystals highlights that they are characterized with a relatively constant chemical composition: 46–54 wt% iron oxides, 28–33% chromium oxides, 13–16% MgO, 2–3% Al_2O_3 and 1–2% NiO.

The morphology of main glassy matrix of sample $GC_{0\text{-}1}$ at high magnification is shown in Fig. 7b. Considering that the crystallinity is very low, this structure might be attributed to a binodal liquid–liquid separation [51]. The nucleation treatment of 1 h at 650 °C does not increase the crystallinity, but the size of the dispersed phase in the glassy matrix decreases and its total amount increases. This might be explained by a continuous immiscibility process during the nucleation treatment. Somewhat similar results are reported also for other silicate systems [41,51].

Another interesting observation is that around the preliminary formed spinel a homogeneous zones around 3–6 μm are formed, as well as that away from these crystals the non-homogeneity of the matrix becomes finer and finer. A possible explanation for these variations in the glassy structure is the creation of a diffusion field around the spinel crystals. These features are highlighted in Image 7-c, which demonstrates a preliminary spinel crystal and the surrounded amorphous phase in sample $GC_{60\text{-}1}$. Fig. 7d elucidates a zone, which is relatively close to the spinel crystal at high magnification and where the amount of the separated phase is lower. It is well seen that this secondary phase has a spherical shape and average size of 80–150 nm. The BEC observations clear highlight that it is enriched of heavy elements.

After 5 min treatment at 730 °C a significant change in size and composition of the preliminary spinel is not observed, which confirm that these crystals are formed mainly during the cooling of the melt. However, the start of pyroxene crystallization in the main glassy matrix also can be evaluated. The formation of a typical dendritic pyroxene crystal in sample $GC_{0\text{-}5}$ is shown in Fig. 8a, while Fig. 8b demonstrates the growth of several pyroxenes on enriched of iron oxides crystal. The EDS analyses elucidate that these new "nuclei" are chromium free and have olivine composition corresponding to fayalite-forsterite solid solutions (i.e. $Fe_{2-x}Mg_xSiO_4$ with x value between 0.6 and 0.8). Early stages of epitaxial growth of pyroxenes on some of the preliminary spinel are also observed.

After 1 h crystallization at 730 °C the phase formation in sample $GC_{60\text{-}60}$ is practically completed. In this sample the epitaxial formation of pyroxene is very well distinguished. This is highlighted in Fig. 9a (BEC) and b (SEI), which demonstrate the growth of individual 0.5–1 μm pyroxene crystals on the preliminary spinel, as well as formation of fine pyroxenes in the surrounded zone. Tiny areas with size of 0.1–0.2 μm and higher concentration of heavy metals also can be distinguished in this region; these formations eventually might be qualified as "secondary" spinel. Here, it can be noted that the epitaxial pyroxene growth is typical for this type of glass-ceramics [18,32], as well as for other similar systems [52–54].

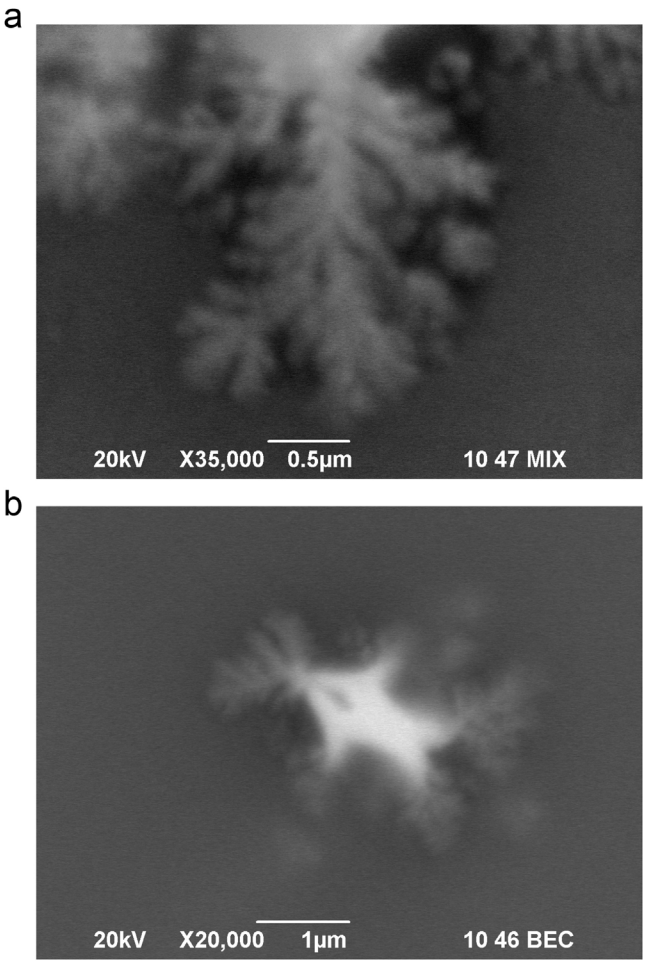

Fig. 8. SEM images after 5 min crystallization at 730 °C (***a*** **-** sample $GC_{0\text{-}5}$; ***c*** and ***d*** –sample $GC_{60\text{-}5}$).

The main structure of glass-ceramics $GC_{60\text{-}60}$ is shown in Fig. 9c. This arrangement is comparable to one of the pyroxene area around the preliminary spinel, but due to the very low dimensions of the crystals and high crystallinity it is difficult to distinguish individual crystals. The formation of some olivine crystals, which are well distinguish due to their higher density, is also manifested.

In sample $GC_{0\text{-}60}$ the crystallization is not totally completed and the pyroxene crystals, both formed by epitaxial growth on preliminary spinel or in the main bulk of samples, are

Table 3
Properties of final glass-ceramic.

Properties	
Density (g/cm^3)	3.16 ± 0.01
Coefficient of thermal expansion in interval 20–400 °C (10^{-7}/C)	70.8 ± 0.1
Bending strength (MPa)	120 ± 9
Compressive strength	250 ± 17
Young's modulus (GPa)	40 ± 2
Hardness (GPa)	9 ± 0.2
Fracture toughness (MPa m$^{1/2}$)	1.6 ± 0.1

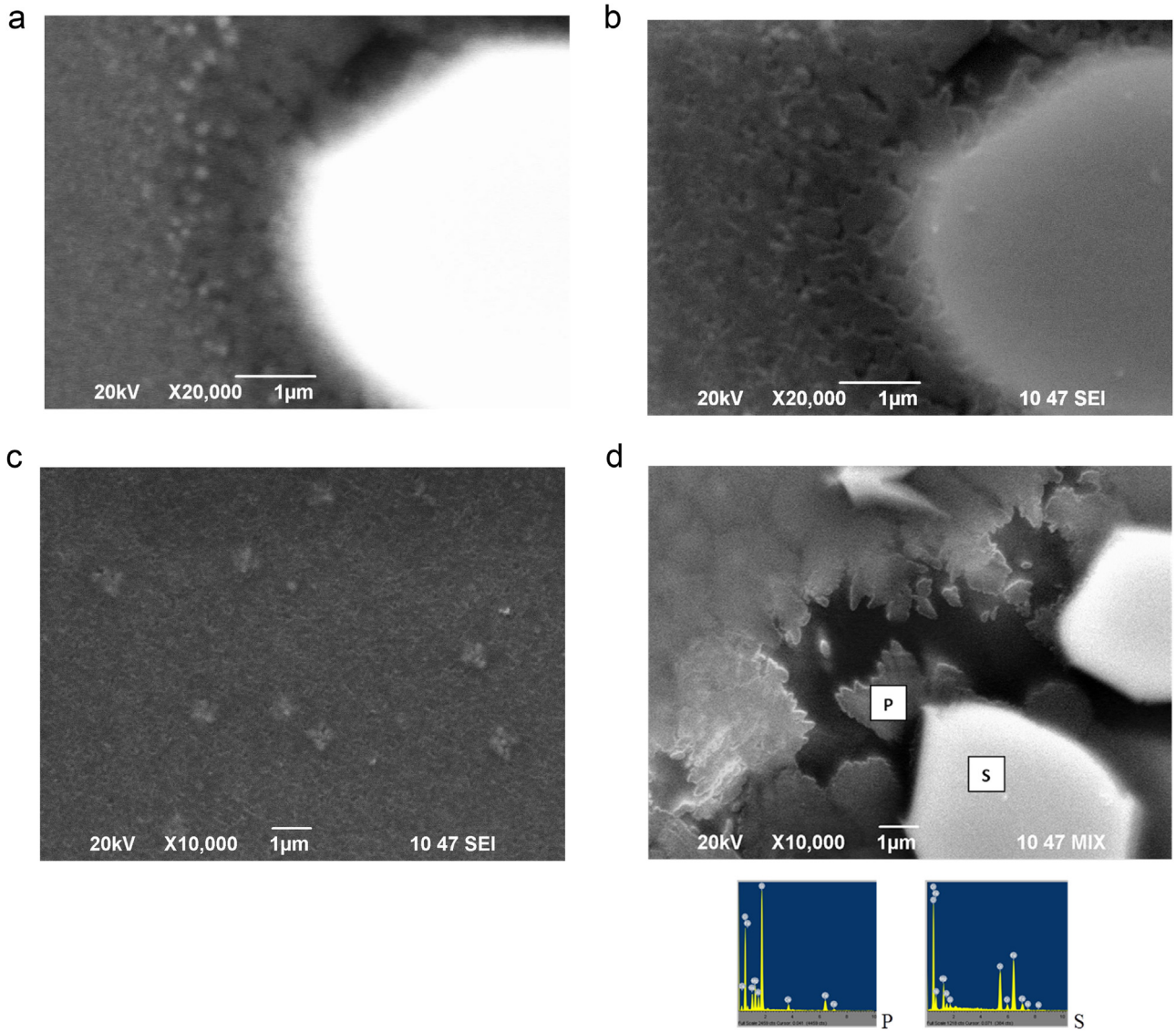

Fig. 9. SEM images after 60 min crystallization at 730 °C (***a, b*** and ***c*** – sample $GC_{60\text{-}60}$; ***d*** –sample $GC_{0\text{-}60}$).

characterized by higher dimensions, reaching 3–6 μm. This is shown in Fig. 9d, where the EDS spectra of main spinel and pyroxene crystal phases are also presented.

The electron microscopy analysis entirely confirms the previous results [42] and suggests that the studied glass-ceramics can be manufactured by a two-step heat-treatment. In this manner, material with higher crystallinity and finer crystalline structure is obtained, which is a premise for good mechanical characteristics.

4.3. Properties of final glass-ceramic

The main characteristics of the glass-ceramic samples, obtained after 1 h nucleation and 1 h crystal growth, were evaluated by different techniques. The results are summarized in Table 3, while the TCLP results of parent glass and final glass-ceramics are compared with ones of the parent wastes in Table 2.

Due to the formation of crystal phases with high density (as iron rich pyroxenes, spinel and olivine) the density of glass-ceramic is slightly higher than ones of the common glass-ceramics by industrial waste [1–3]. At the same time, the coefficient of thermal expansion is moderate and even a little lower than these of the typical waste glass-ceramics for building or tiling application. This value is comparable with the expected coefficients of thermal expansion of both main crystal phases [55–57] and with ones of residual low alkali glassy phase (estimated by the Appen methods [39]). This elucidates that the formation of significant stresses in the material are not expected.

The obtained glass-ceramic is characterized with enhanced hardness and high bending strength, as well as with a compressive strength and Young modulus similar to other iron-reach glass-ceramics [13]. Such good mechanical characteristics can be explained by the structure of the material. In fact, the main crystalline phase in the material is pyroxene, which is characterized with high hardness, while the crystallites size is below 1 μm, which is prerequisite for good bending strength. In addition, this small-sized structure implies higher surface area of the contact planes between the crystals, which increases the capacity of the material to accumulate mechanical energy.

The value of fracture toughness also is elevated. The obtained relatively high value [58] is result not only of the structure, but also of the origin and the propagation of cracks. As it is shown in Fig. 10, the cracks originate from the corners and the edges of the indentation and interrupt after relatively shorter path of propagation.

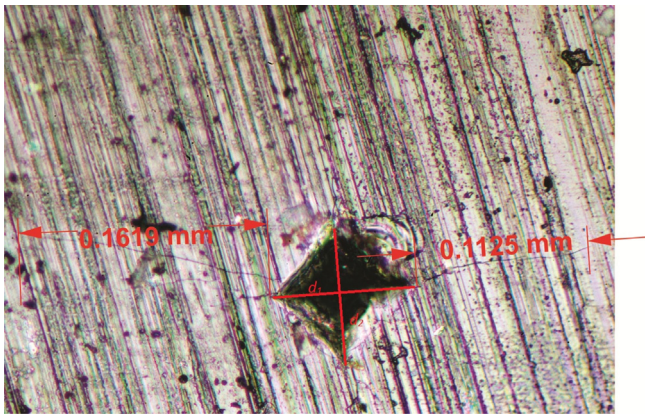

Fig. 10. Optical microscopy images after indentation test.

Finally, the TCLP test of the parent glass and the final glass-ceramics clearly elucidate that the obtained materials are completely inert (see Table 2). The concentration of the measured heavy metals decreases by two to four orders in comparison with the values for the initial hazardous wastes. Therefore the vitrification of the used metallurgical waste materials is an effective way to capture the heavy metals and to avoid the negative impact on the environment.

5. Conclusions

The possibilities to manufacture glass-ceramics by sinter-crystallization or bulk crystallization using glass, based on 70 wt % hazardous wastes from the ferronickel smelting plant, are studied.

The parent glass is characterized by a very high crystallization trend, which is a consequence of elevated amounts of chromium oxides, iron oxides and magnesium oxides in the composition. As a result, the sintering process is totally inhibited by the intensive phase formation, which compromises the sinter-crystallization method. At the same time, fine crystalline bulk glass-ceramic are obtained after a short low-cost thermal cycle: 45–60 min nucleation at 650 °C and 30–60 min crystallization at about 730–750 °C.

The crystallization process is peculiar, which leads to a complex structure of the material. The phase formation starts during the melt cooling with the precipitation of preliminary Fe-Mg-Cr spinel crystals. Then, these crystals act as centers for epitaxial growth of pyroxene phase, forming a part of the glass-ceramic arrangement. However, the main structure is a result of the tendency for liquid–liquid immiscibility, which leads to the formation of 0.5–1.0 μm pyroxenes as a main crystal phase. The crystallization of some tiny olivine crystals, also acting as nuclei for pyroxene growth, is furthermore noted.

The obtained glass-ceramic is characterized as an inert material with a high chemical durability and very good exploitation characteristics.

References

[1] I.W. Donald, Waste Immobilization in Glass and Ceramic Based Hosts: Radioactive, Toxic, and Hazardous Wastes, John Wiley & Sons, 2010.
[2] R.D. Rawlings, J.P. Wu, A.R. Boccaccini, Glass-ceramics: their production from wastes–a review, J. Mater. Sci. 41 (2006) 733–761.
[3] P. Colombo, G. Brusatin, E. Bernardo, G. Scarinci, Inertization and reuse of waste materials by vitrification and fabrication of glass-based products, Curr. Opin. Solid State Mater. 7 (2003) 225–239.
[4] A. López-Delgado, H. Tayibi, C. Pérez, F.J. Alguacil, F.A. López, A hazardous waste from secondary aluminium metallurgy as a new raw material for calcium aluminate glasses, J. Hazard. Mater. 165 (2009) 180–186.
[5] E. Bernardo, L. Esposito, E. Rambaldi, A. Tucci, Y. Pontikes, G.N. Angelopoulos, Sintered esseneite-wollastonite-plagioclase glass-ceramics from vitrified waste, J. Eur. Ceram. Soc. 29 (2009) 2921–2927.
[6] T. Yu, Z. Wei, C. Dongdong, Crystallization evolution, microstructure and properties of sewage sludge-based glass-ceramics prepared by microwave heating, J. Hazard. Mater. 196 (2011) 370–379.
[7] J.A. Roether, D.J. Daniel, D. Amutha Rani, D.E. Deegan, C.R. Cheeseman, A.R. Boccaccini, Properties of sintered glass-ceramics prepared from plasma vitrified air pollution control residues, J. Hazard. Mater. 173 (2010) 563–569.
[8] P. Kavouras, E. Pantazopoulou, S. Varitis, G. Vourlias, K. Chrissafis, G.P. Dimitrakopulos, M. Mitrakas, A.I. Zouboulis, Th. Karakostas, A. Xenidis, Incineration of tannery sludge under oxic and anoxic conditions: study of chromium speciation, J. Hazard. Mater. 283 (2015) 672–679.
[9] E.B. Ferreira, E.D. Zanotto, L.A.M. Scudeller, Glass and glass-ceramic from basic oxygen furnace (BOF) slag, Glass Sci. Technol. 75 (2002) 75–86.
[10] L. Barbieri, A.C. Bonamartini, I. Lancellotti, Alkaline and alkaline-earth silicate glasses and glass-ceramics from municipal and industrial wastes, J. Eur. Ceram. Soc. 20 (2000) 2477–2483.
[11] G.A. Khater, Influence of Cr_2O_3, LiF, CaF_2 and TiO_2 nucleants on the crystallization behavior and microstructure of glass-ceramics based on blast-furnace slag, Ceram. Int. 37 (2011) 2193–2199 (PAK za Cr).
[12] T.W. Cheng, T.H. Ueng, Y.S. Chen, J.P. Chiu, Production of glass-ceramic from incinerator fly ash, Ceram. Int. 28 (2002) 779–783.
[13] L. Baowei, D. Yongsheng, Z. Xuefeng, Z. Ming, C. Hua, Crystallization characteristics and properties of high-performance glass-ceramics derived from baiyunebo east mine tailing, Environ. Prog. Sustain. Energy 34 (2015) 420–426.
[14] R.K. Chinnam, A.A. Francis, J. Will, E. Bernardo, A.R. Boccaccini, Review. Functional glasses and glass-ceramics derived from iron rich waste and combination of industrial residues, J. Non Cryst. Solids 365 (2013) 63–74.
[15] M. Pelino, C. Cantalini, J. Ma Rincon, Preparation and properties of glass-ceramic materials obtained by recycling goethite industrial waste, J. Mater. Sci. 32 (1997) 4655–4660.
[16] M. Romero, J. Ma Rincon, Preparation and properties of high iron oxide content glasses obtained from industrial wastes, J. Eur. Ceram. Soc. 18 (1998) 153–160.
[17] A. Karamanov, P. Pisciella, M. Pelino, The effect of Cr_2O_3 as a nucleating agent in iron rich glass-ceramics, J. Eur. Ceram. Soc. 19 (1999) 2641–2645.
[18] M. Romero, J. Ma Rincón, Surface and bulk crystallization of glass-ceramic in the na2O-CaO-ZnOPbO-Fe2O3-Al2O3-SiO2 system derived from a goethite waste, J. Am. Ceram. Soc. 82 (1999) 1313–1317.
[19] A. Karamanov, M. Pelino, Crystallization phenomena in iron-rich glasses, J. Non Cryst. Solids 281 (2001) 139–152.
[20] P. Kavouras, T. Kehagias, I. Tsilika, G. Kaimakamis, K. Chrissafis, S. Kokkou, D. Papadopoulos, Th. Karakostas, Glass-ceramic materials from electric arc furnace dust, J. Hazard. Mater. 139 (2007) 424–429.
[21] A. Karamanov, M. Aloisi, M. Pelino, Vitrification of copper flotation waste, J. Hazard. Mater. 140 (2007) 333–339.
[22] S. Çoruh, O.N. Ergun, Leaching characteristics of copper flotation waste before and after vitrification, J. Environ. Manage. 81 (2006) 333–338.
[23] A. Karamanov, L.M. Schabbach, E. Karamanova, F. Andreola, L. Barbieri, B. Ranguelov, G. Avdeev, I. Lancellotti, Sinter-crystallization in air and inert atmospheres of a glass from pre-treated municipal solid waste bottom ashes, J. Non Cryst. Solids 389 (2014) 50–59.
[24] Y.B. Zong, Z.B. Liu, J.J. Hou, H.X. Li, Investigation of glass-ceramics based on steel slag under various sintering atmospheres, Adv. Mater. Res. 1065 (2015) 1784–1790.
[25] S.I. Gutnikov, M.S. Manylov, Ya.V. Lipatov, B.I. Lazoryak, K.V. Pokholok, Effect of the reduction treatment on the basalt continuous fiber crystallization properties, J. Non Cryst. Solids 368 (2013) 45–50.
[26] G.A. Khater, A. Abdel-Motelib, A.W. El Manawi, M.O. Abu Safiah, Glass-ceramics materials from basaltic rocks and some industrial waste, J. Non Cryst. Solids 358 (2012) 1128–1134.
[27] P. Sengupta, A review on immobilization of phosphate containing high level nuclear wastes within glass matrix–present status and future challenges, J. Hazard. Mater. 235–236 (2012) 17–28.
[28] M.I. Ojovan, W.E. Lee, An Introduction to Nuclear Waste Immobilisation, Elsevier, 2005.
[29] A. Karamanov, R. Di Gioacchino, P. Pisciella, M. Pelino, S. Hreglich, Viscosity of iron-rich glasses from industrial wastes, Glass Technol. 43 (2002) 34–38.
[30] H. Scholze, Glass Nature, Structure and Properties, Springer-Verlag, Berlin, 1991.
[31] J.E. Shelby, Introduction to Glass Science and Technology, Second Edition, The Royal Society of Chemistry, Cambridge, UK, 2005.
[32] W. Holand, G. Beall, Glass-Ceramics Technology, The American Ceramics Society, Westerville, 2002.
[33] R. Harizanova, G. Völksch, C. Rüssel, Microstructures formed during devitrification of Na_2O. Al_2O_3. B_2O_3. SiO_2. Fe_2O_3 glasses, J. Mater. Sci. 45 (2010) 1350–1353.
[34] V.K. Marghousian, S. Arjomandnia, Effect of Cr_2O_3 on nucleation of SiO_2-Al_2O_3-CaO-MgO-(R_2O, Fe_2O_3, TiO_2) glass-ceramics, Phys. Chem. Glasses 39 (1998) 246–251.
[35] R.D. Rawlings, Production and properties of silceram glass-ceramics. In Glass-Ceramic Materials –Fundamentals and Applications Series of Monographs on Material Science, Engineering and Technology, Mucchi Editore, Ed. Rinkon LMa, Modena 1997, pp. 115–133.

[36] L. Barbieri, C. Leonelli, T. Manfredini, G.C. Pellacani, C. Siligardi, E. Tondello, R. Bertoncello, Solubility, reactivity and nucleation effect of Cr_2O_3 in the CaO-MgO-Al_2O_3-SiO_2 glassy system, J. Mater. Sci. 29 (1994) 6273–6280.
[37] H. Khedim, T. Katrina, R. Podor, P. Panteix, C. Rapin, M. Vilasi, Solubility of Cr_2O_3 and speciation of chromium in soda–lime–silicate melts, J. Am. Ceram. Soc. 93 (2010) 1347–1354.
[38] H. Khedim, R. Podor, C. Rapin, M. Vilasi, Redox-control solubility of chromium oxide in soda-silicate melts, Am. Ceram. Soc. 91 (2008) 3571–3579.
[39] A.A. Appen, Chemistry of glass, Chemistry, Lenigrad, 1974.
[40] I. Gutzow, J. Schmelzer, The Vitreus State, Thermodynamics, Structure, Rheology and Crystallization, Springer-Verlag, Berlin, 1995.
[41] J. Ma Rincón, C.J.R. González-Oliver, P.F. James, Phase separation in Li_2O-SiO_2 glasses with additions of V_2O_5, MnO_2 and Cr_2O_3, J. Mater. Sci. 23 (1988) 2512–2516.
[42] E. Ljatifi, A. Kamusheva, A. Grozdanov, P. Paunović, A. Karamanov, Optimal thermal cycle for production of glass-ceramic based on wastes from ferronickel manufacture, Ceram. Int. 41 (2015) 11379–11386.
[43] EN 12457-2. Characterization of waste. Leaching compliance test for leaching of granular waste materials and sludge; 2002.
[44] J.B. Wachtman, W.R. Cannon, M.J. Matthewson, Mechanical Properties of Ceramics, John Wiley & Sons, Inc, New Jersey, 2009.
[45] B.P. Lawn, E.P. Fuller, Equilibrium penny-like cracks in indentation fracture, . Mater. Sci. 10 (1975) 2016–2024.
[46] Y. Yue, Characteristic temperatures of enthalpy relaxation in glass, J. Non Cryst. Solids 354 (2008) 1112–1118.
[47] P.M. Sørensen, M. Pind, Y.Z. Yue, R.D. Rawlings, A.R. Boccaccini, E.R. Nielsen, Effect of the redox state and concentration of iron on the crystallization behavior of iron-rich aluminosilicate glasses, J. Non Cryst. Solids 351 (2005) 1246.
[48] A. Karamanov, Vitrification and sinter-crystallization of iron-rich industrial wastes, Adv. Sci. Technol. 92 (2014) 174–183.
[49] A.R. Boccaccini, B. Hamann, In-situ high temperature optical microscopy. A review, J. Mater. Sci. 34 (1999) 5419–5436.
[50] J. Pascual, A. Duran, M.O. Prado, A new method for determining fixed viscosity points of glasses, Phys. Chem. Glasses 46 (2005) 12–20.
[51] W. Vogel, Glass Chemistry, Second Edition, Springer-Verlag, Berlin, 1994.
[52] J.E. Hammer, T.G. Sharp, P. Wessel, Heterogeneous nucleation and epitaxial crystal growth of magmatic minerals, Geology 38 (4) (2010) 367–370.
[53] G. Kaur, Solid Oxide Fuel Cell Components: Interfacial Compatibility of SOFC Glass Seals, Springer, New York, 2016.
[54] W. Deer, R.A. Howie, J. Zussman, Introduction to the Rock-Forming Minerals, Longman Scientific and Technical, New York, 1992.
[55] L. Cartz, J.D. Jorgensen, Pressure and temperature behavior of frame work silicates and nitrides, in: D.C. Larsen (Ed.), Thermal Expansion, Premium Press, New York, 1982, pp. 147–156.
[56] J. Haselton, B.S. Hemingway, R.A. Robie, Low temperature heat capacities of $CaAl_2SiO_6$ glass and pyroxene and thermal expansion of $CaAl_2SiO_6$ pyroxene, Am. Mineral. 69 (1984) 489–493.
[57] S.N. Salama, E.A. Saad, H. Darwish, H.A. Abo-Mosallam, Formation of glass-ceramic materials based on pyroxene solid solution—fluorapatite phases and their thermal expansion properties, Ceram. Int. 31 (2005) 559–566.
[58] W. Han, Glass ceramic of high hardness and fracture toughness developed from iron-rich wastes, Acta Metall. Sin. (Engl. Lett.) 22 (2009) 181–190.